Influence of extrusion 4D printing parameters on the thermal shape-morphing behaviors of polylactic acid (PLA)

Aref Ansaripour[a], Mohammad Heidari-Rarani[a,*], Rasoul Mahshid[a], Mahdi Bodaghi[b]

[a]Department of Mechanical Engineering, Faculty of Engineering, University of Isfahan, 81746-73441 Isfahan, Iran

[b]Department of Engineering, School of Science and Technology, Nottingham Trent University, Nottingham NG11 8NS, United Kingdom

*Corresponding author: m.heidarirarani@eng.ui.ac.ir

Abstract

A simple and inactive structure is able to transform into a complex and active one via four-dimensional (4D) printing. Controlling bending deformation, activation time, and temperature is crucial in 4D printing. This study aimed to comprehensively evaluate and analyze the effect of different process parameters on the bending deformation of polylactic acid (PLA) shape-morphing produced by material extrusion additive manufacturing. These parameters included layup, layer thickness, printing speed, nozzle temperature, nozzle diameter, and bed temperature. Since the bending deformation is significantly affected by the specimen wall, this study has focused, for the first time, on the simultaneous influence of process parameters and presence of a wall on the deformation. Furthermore, the study examined the influence of printing parameters on activation time and activation temperature. The results indicated that increasing the pre-strain stored in the parts led to a decrease in activation time and activation temperature. Subsequently, the the Taguchi design of experiment method was used to optimize the most influential parameters on the bending deformation. The difference between the optimal predicted and the experimental deformations was less than 2%. Layer thickness, layup, nozzle temperature, and printing speed were recognized respectively as the most effective parameters for controlling deformation.

Keywords: 4D printing; Fused deposition modeling; Material extrusion; Polylactic acid; Thermal stimulus; Taguchi design.

1 Introduction

Additive manufacturing (AM) or three-dimensional (3D) printing is a general term for various manufacturing methods that aim to create structures based on stacking layers on top of each other to create complex 3D geometries. Its main features include freedom in designing structures, minimizing materials lost, rapid prototyping, and building structures with complex geometries [1–3]. According to ISO/ASTM 52900, seven procedures have been introduced for additive manufacturing of polymers in which the most common one is material extrusion [4, 5]. Material extrusion method has different ways to create parts. One of them is the fused deposition modeling (FDM) method, which is also known as fused filament fabrication (FFF). This method is the most common method for additive manufacturing of thermoplastic polymers [6–8]. FFF printers create various structures layer by layer from a 3D computer model by heating filaments of thermoplastic polymers, converting them into a semi-liquid state, and extruding them through a small nozzle to print the complete specimen [9, 10]. Fig. 1 illustrates a general schematic of the FFF process.

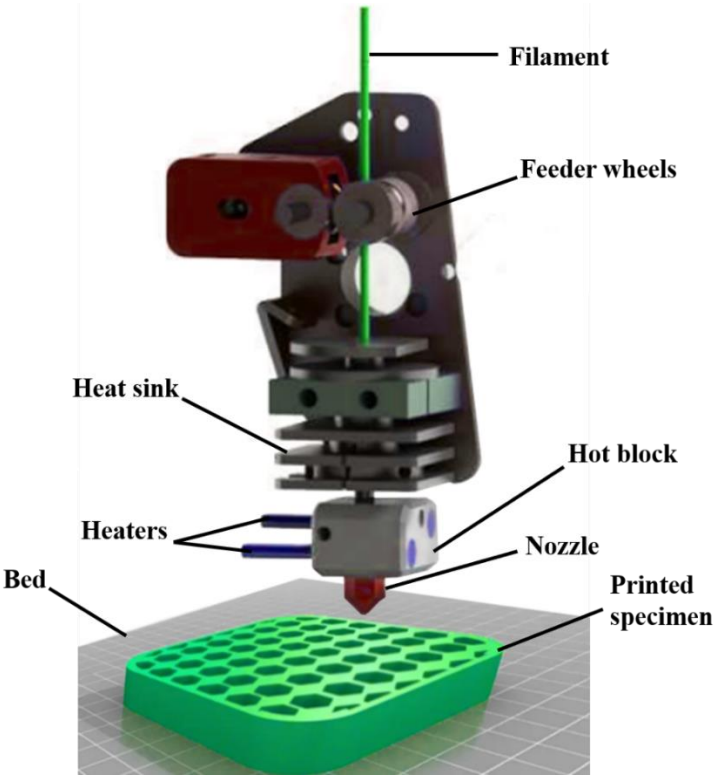

Fig. 1 A schematic of the FFF process

By enhancing materials science, the 3D printing approach has been developed and upgraded to four-dimensional (4D) printing [11]. With the definition of 4D printing in 2013, a lot of attention has been

attracted to this field, resulting from the interdisciplinary research and growth of smart materials, 3D printers, and design [12]. 4D printing is based on 3D printing, which requires additional stimuli (such as heat [13], water [14], PH [15], etc.) and stimuli-responsive materials that evolve as a function of time based on specific interaction mechanisms between smart materials and stimuli [16]. With the advancements of 4D printing, this printing technique has been able to spread in various fields such as medicine [17], metamaterials [18], aerospace [19], sensors [20], soft robotics [21], and automotive [22]. Smart materials include various materials, for instance, shape memory polymers (SMPs) [23], hydrogels [24], and shape memory alloys (SMAs) [25]. SMPs are typically smart soft materials that have the ability to transform from a temporary configuration to their initial configuration in response to external stimuli [26]. Polylactic acid (PLA) is a common SMP in 3D and 4D printing used in FFF printers [27]. Nowadays, due to the fact that the use of petroleum products has expanded significantly and causes long-term risks for the ecosystem, in this regard, replacing synthetic polymers with biological and biodegradable polymers is a suitable strategy to deal with this issue. PLA, which is comparable in performance to petroleum-based polymers, is a biodegradable polymer that is widely used in medical applications [28, 29].

Due to the expansion of 4D printing in various industries, it is essential to know the behavior of materials, stimuli, and the effects of manufacturing parameters on the bending deformation and activation time of structures. Bending deformation behavior applies to special fields such as gripes [30], stents [31], hinges [32], self-assembly structures [33], and tissue engineering [34], and some studies were conducted on this behavior. For this purpose, Hu et al. [35] used a thermally-responsive shape memory polymer with self-bending characteristics without any need for prior programming in disk, ring, and strip-shaped structures using an FFF 3D printer. Bodaghi et al. [36] investigated experimentally and numerically the efficacies of printing speed on the bending specifications of PLA specimens. Their results indicated that by heating the printed specimen up to the glass transition temperature (T_g), larger deformations can be achieved by increasing the printing speed. Manen et al. [37] inquired about the layer thickness effect on the activation time. It was found that the activation time can be controlled by changing the layer thickness. Bodaghi et al. [38] perused the influence of printing temperature at two levels of 210°C and 230°C on an SMP. Their results showed that the amount of deformation decreases with the increase in printing temperature. They explained the reason for this phenomenon in the way that any increase in printing temperature has an inverse effect on the pre-strain stored during printing and reduces the amount of deformation in response to the applied stimulus. Kacergis et al. [39] studied the behavior of printed structures made of PLA and TPU. The printed layers of PLA played the role of active layers in the printed structures. They examined the influence of three parameters including the number of active layers, printing speed, and bed

temperature in these structures. Their results demonstrated that by heating the printed specimens in water at 85°C for 2 minutes, the specimens fabricated with a higher printing speed had more deformation and the specimens printed with a lower bed temperature deformed more. In another study, Yu et al. [40] printed two-component structures including PLA as the active block and carbon fiber-reinforced polylactic acid (CFPLA) as the limited block to strengthen the structures. They studied the three printing factors including printing orientation, layer thickness, and material characteristics. It was found that by enhancing the layer thickness, the value of deformation declined due to applying a stimulus, and the deformation could be controlled by the orientation of the layers. Research in the field of 4D printing was not limited to using shape memory polymers. Goo et al. [41] perused the impact of the layering procedure on the thermal bending deformation of acrylonitrile butadiene styrene (ABS) without shape memory effect by making anisotropy in the printing orientations. Their results displayed that much more flexural deformation can be achieved compared to homogeneous layering. Tezerjani et al. [42] proposed a model for circular disks fabricated from PLA using the response surface method. Their variable parameters included printing speed, layer thickness, bed temperature, and nozzle temperature. The results of this study revealed that by optimizing the printing parameters, the maximum deformation of the circular disc is 17.63 mm. Recently, Alshebly et al. [43] investigated the filling patterns and percentage of filling on a SMP. They stated that variable stiffness can be utilized to program the shape memory effect (SME) of structures in different ways.

The above literature review indicates that limited attention has been given to the impact of layup, nozzle diameter, bed temperature, and specimen wall on the bending deformation in 4D printing. In this study, a comprehensive investigation of all process parameters was conducted for the first time on two types of specimens, with and without wall. The one-factor-at-a-time (OFAT) method was employed for the recognition of effective parameters of 3D-printed PLA shape-morphing specimens using an FFF printer. Additionally, this study examined the influence of print parameters on activation time and activation temperature. Finally, the significant parameters were identified, and optimization was performed using the Taguchi design of experiment method.

2 Material and method

2.1 Materials

The PLA+ filament provided by eSUN company has been utilized to fabricate the specimens. In order to obtain polylactic acid melting point and T_g, the differential scanning calorimetry (DSC) test was done on PLA filament from 24 to 240°C at a rate of 10°C⁄min. Fig. 2 shows the DSC test results. The melting

temperature and T_g are approximately 171˚C and 57˚C, respectively. To determine the T_g value, the average of the initial drop range (50˚C to 64˚C) was considered as depicted in Fig. 2.

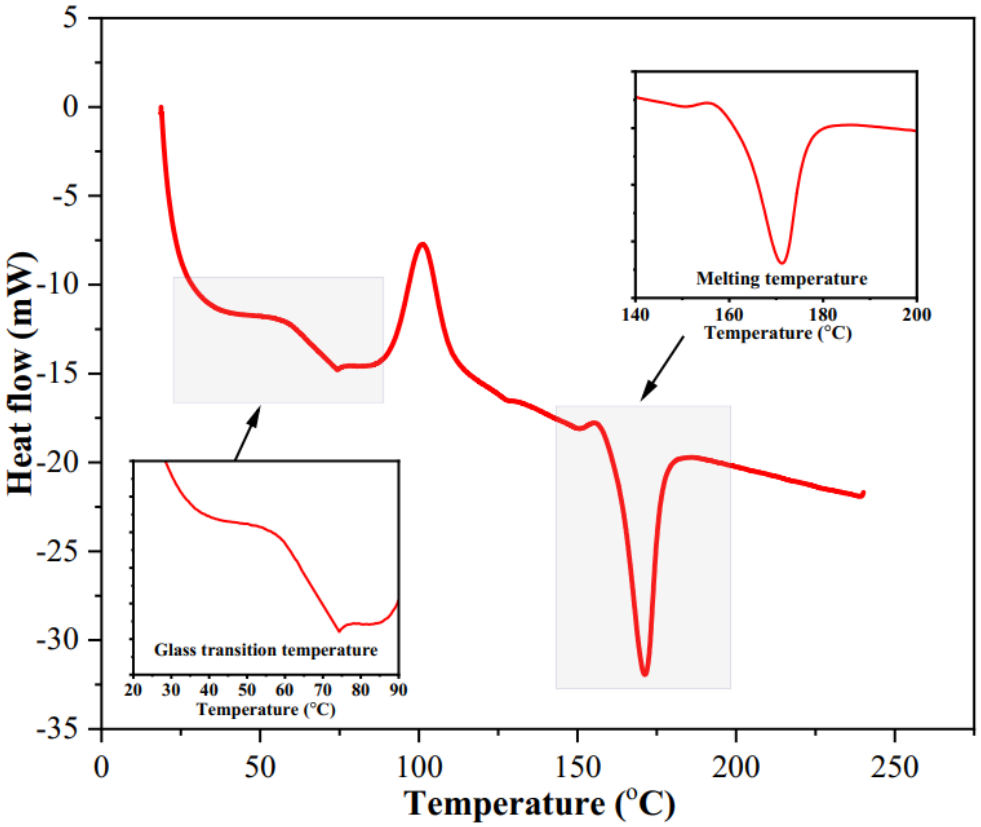

Fig. 2 DSC test for PLA filament

2.2 Specimen preparation

The 3D model of the parts is designed by SOLIDWORKS software with the dimensions of 90 mm ×12 mm ×1.2 mm and 110 mm ×12 mm ×1.2 mm. The standard triangle language (STL) output was taken from the software and imported to Cura software to determine the printing parameters. The constant printing parameters are reported in Table 1. The G-code output of Cura software is given to the 3D printer to print the specimens.

Specimens with the dimensions of 90 mm × 12 mm × 1.2 mm were printed with three walls in order to examine the effect of wall parameters and non-uniform speed on the printing process. To remove the influence of the wall and non-uniform speed, specimens measuring 110 mm × 12 mm × 1.2 were cut using a surgical blade and resized to dimensions of 90 mm × 12 mm × 1.2 mm. The non-uniformity of speed refers to the phenomenon where the nozzle reduces its speed as it approaches the end of its trajectory. As a result, there are variations in speed between the middle and the edges of the specimen.

Table 1 Constant printing parameters

Process parameters	Value
Print speed, mm/s	60
Nozzle diameter, mm	0.4
Layer thickness, mm	0.1
Nozzle temperature, ˚C	190
Bed temperature, ˚C	30
Infill density, %	100

2.3 Test procedure

The heat stimulus was applied by an oven from the ambient temperature up to 30˚C higher than T_g, i.e., 87˚C for 40 minutes. The length of the specimens was measured before and after applying the stimulus with a caliper with a resolution of 0.01 mm. Fig. 3 shows how to measure the distance between the two ends of the specimens before and after applying the stimulus. All specimens initially have a length of L_0, and after applying the thermal stimulus, their length will reach L_f. The percentage of the bending deformation rate of the specimens is calculated from Eq. (1).

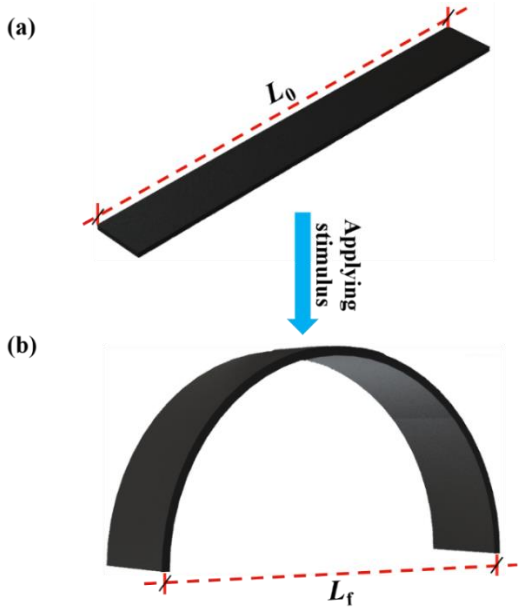

Fig. 3 (a) Primary length of L_0 before applying the stimulus and (b) Secondary length of L_f after applying the stimulus

$$\text{Deformation percentage} = \frac{L_f - L_0}{L_0} \times 100 \quad (1)$$

In order to recognize that the obtained results in this research are reliable, three series of specimens have been printed and tested. Ten stacking sequences with different permutations of angles of 0° (in the direction of the specimen lenght) and 90° (in the direction of the specimen width) have been investigated. Fig. 4 shows the orientation of 0° and 90° in the printed specimens.

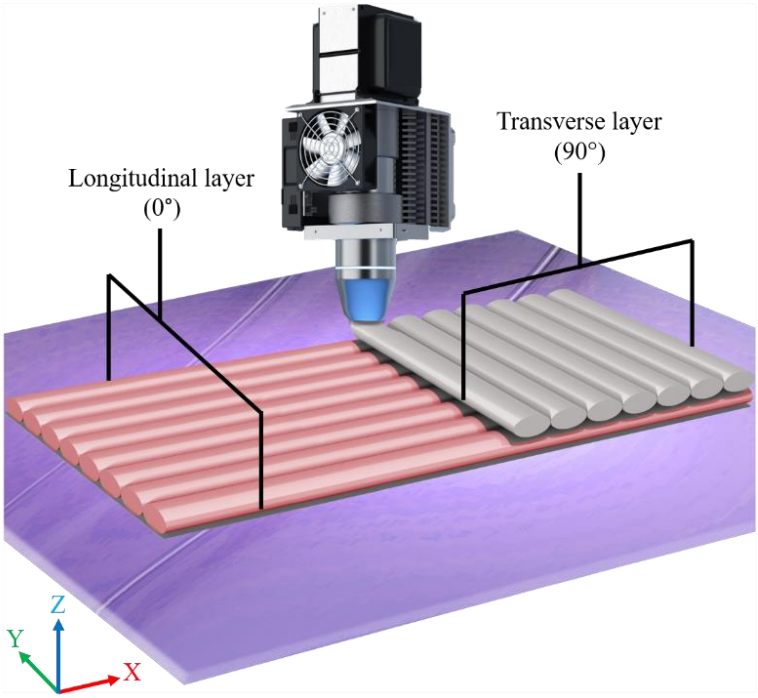

Fig. 4 Orientation of the layer with an angle of 90° along the width of the specimen and orientation of the layer with an angle of 0° along the length of the specimen

2.4 Design of experiment (DOE) procedure

In the process of designing experiments, specific input parameters, known as independent variables, are randomly selected. These experiments are then carried out to generate results, which act as output parameters or dependent variables within the framework of the DOE method. These obtained results are subsequently utilized for the parameter optimization. One approach for optimizing the output parameters involves the implementation of response surface methodology, which is a particular type of DOE that aids in predicting the output parameters. Another technique is the use of the mixture design of experiment, which helps identify the optimal combination of composite materials to achieve the highest response. Additionally, the Taguchi DOE method is another strategy employed to optimize the input parameters and attain maximum values for the output parameters.

The main purpose of this study is to optimize the level of effective parameters on the bending deformation of 3D-printed PLA materials having no walls. Thus, utilizing Minitab software, the Taguchi method is utilized to obtain the best level of parameters. Four effective parameters are selected for the optimization process via the Taguchi method and an L18 Taguchi orthogonal array is designed and reported in Table 2. The mixed-level design is applied for the optimization of parameters (three parameters in three levels and one parameter in two levels). The layups P1, P2, and P3 are $[90_n/0_n]$, $[0_n/90_n]$, and $[0_{2/3n}/90_{1/3n}]$, respectively. These three layups are chosen based on the highest bending deformations occurred for the printed PLA discussed in Section 3.1.1.

Table 2 An L18 Taguchi orthogonal array

Specimen	Layer thickness (mm)	Layup	Nozzle temperature (°C)	Printing speed (mm/s)
1	0.1	P1	190	20
2	0.1	P1	200	40
3	0.1	P1	210	60
4	0.1	P2	190	20
5	0.1	P2	200	40
6	0.1	P2	210	60
7	0.1	P3	190	40
8	0.1	P3	200	60
9	0.1	P3	210	20
10	0.2	P1	190	60
11	0.2	P1	200	20
12	0.2	P1	210	40
13	0.2	P2	190	40
14	0.2	P2	200	60
15	0.2	P2	210	20
16	0.2	P3	190	60
17	0.2	P3	200	20
18	0.2	P3	210	40

3 Results and discussion

3.1 Effect of process parameters

In this section, the effect of the layup on the amount of bending deformation is initially evaluated. Following the evaluation of the layup [$90_n/0_n$], the impact of other parameters is examined to gain a better understanding of the results.

3.1.1 Layup effect

Table 3 indicates ten different layups for 3D printed specimens with permutations of 0° and 90° layers. Regarding the purpose of this study which is the evaluation of bending deformation changes along the length of the specimen, the 0° and 90° layups have been chosen. The specimens were printed according to the default printing conditions of Table 1. Fig. 5 shows the average and standard deviation of bending deformation percentage for specimens without wall. Fig. 6 demonstrates the final deformation of the printed specimens with the layups illustrated in Table 3.

Table 3 The name and layup of each specimen

Specimen name	Layup
A-1	$[90]_{12}$
A-2	$[0]_{12}$
A-3	$[90_6/0_6]$
A-4	$[0_6/90_6]$
A-5	$[90_9/0_3]$
A-6	$[0_9/90_3]$
A-7	[90/0/90/0/90/0/90/0/90/0/90/0]
A-8	[0/90/0/90/0/90/0/90/0/90/0/90]
A-9	[90/0/90/0/90/0] s
A-10	[0/90/0/90/0/90] s

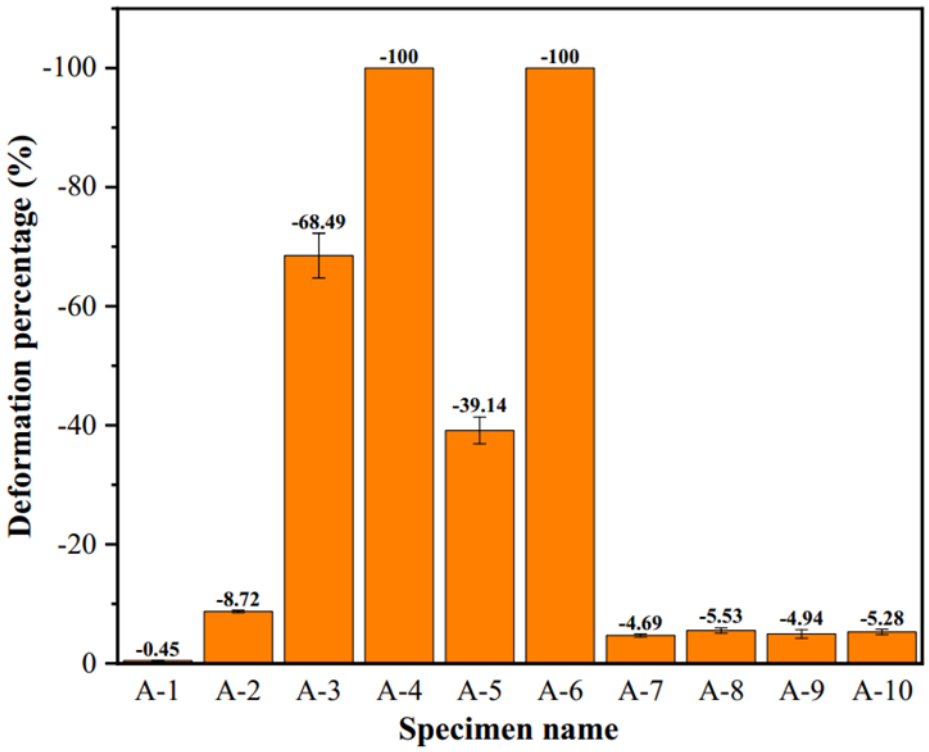

Fig. 5 Bending deformation percentage of different layups

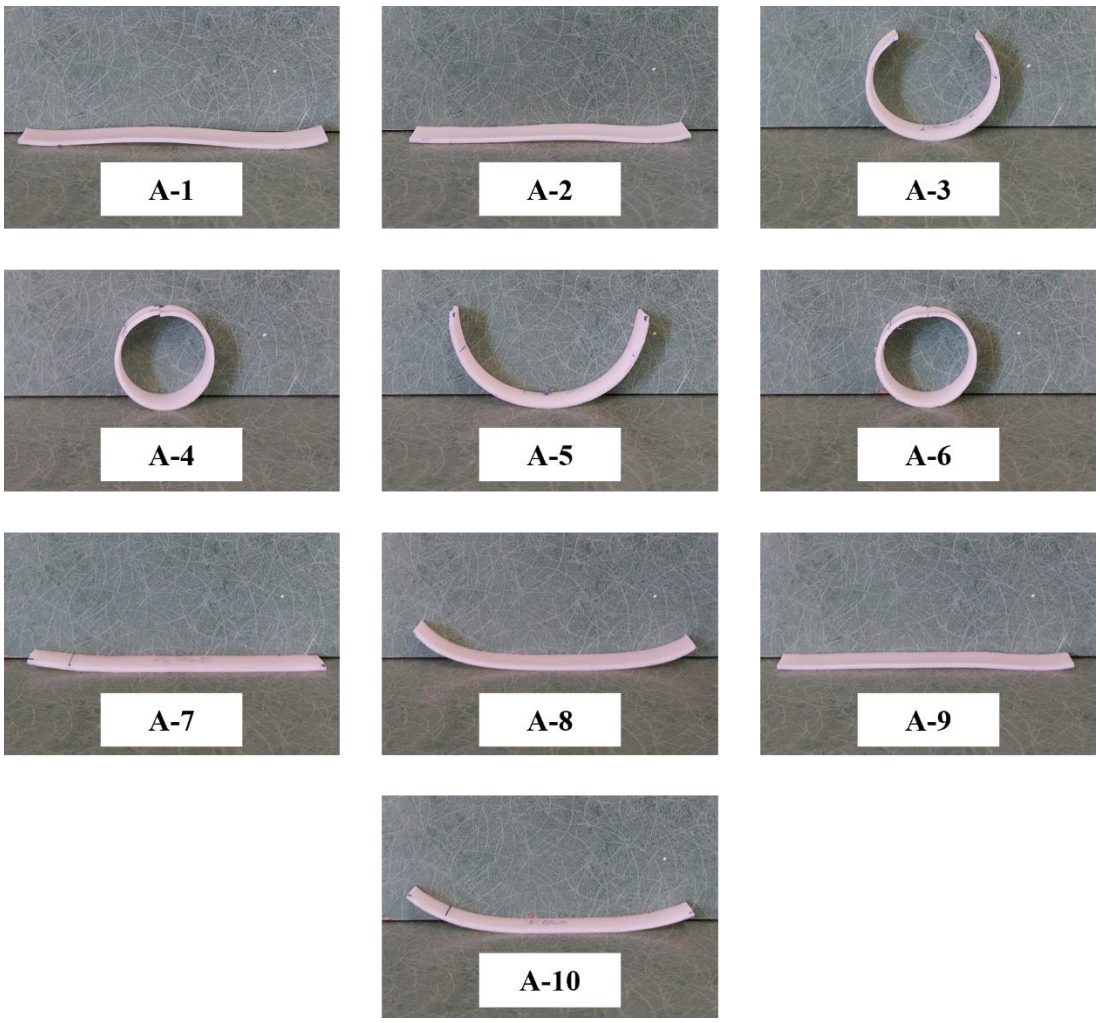

Fig. 6 The final deformation of 3D-printed shape-morphing PLA material with different layups

It can be found from Fig. 5 that the creation of anisotropy in the asymmetric and non-homogeneous layups in the printed specimens is a crucial factor in the bending deformation. In addition, the shrinkage of the longitudinal layers of the specimen when applying stimulus will cause bending in the length direction. For example, the minimum extent of the bending deformation is observed in the symmetric layups such as A-1, A-2, A-9, and A-10 against the asymmetry layering. Assuming symmetric specimens with the same pre-strain applied to the 0° and 90° layers at each position, it can be observed that the shrinkage of the upper 6 layers neutralizes the shrinkage of the lower 6 layers. As a result, these layers exhibit reduced deformation.

Based on the results obtained, it can be concluded that the highest amount of deformation is observed in the asymmetric specimens, except for specimens A-8 and A-7. Samples A-8 and A-7 exhibit less deformation due to a lower level of asymmetry compared to other asymmetric specimens. The

asymmetric specimens A-3, A-4, A-5, and A-6 demonstrate higher levels of deformation, which can be attributed to both their inherent asymmetry and the varying amount of stored pre-strain among their layers. It is worth noting that specimens A-3 and A-4 give different bending results due to the change of the orientation of the longitudinal and transverse layer in the above and bottom of the parts. This discrepancy can be attributed to the different levels of pre-strain stored in each layer. As reported in Ref. [38, 42], each layer possesses a distinct amount of stored pre-strain, with the level of pre-strain increasing as one moves towards the higher layers (see Fig. 7). The reasons behind the pre-strain increases when the specimen height increases are as follows:

- The last layer that is printed has a larger contact surface time with the environment, allowing the layer to exchange more heat received from the FFF printer nozzle with the surrounding environment compared to the lower layers.
- The melted materials coming out of the nozzle give less heat to the layers printed later.
- The top layers will achieve less heat generated by the bed of FFF printer than the lower layers.

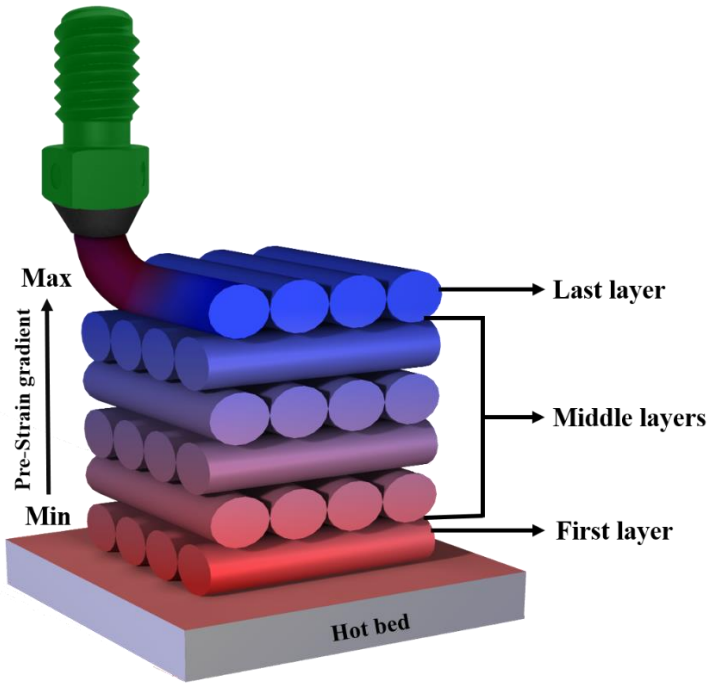

Fig. 7 Gradient of stored pre-strain between layers during printing

In the investigation done by Jamshidi et al. [44] on the strip-shaped PLA specimens, it was found that the most bending deformation occurs at non-homogeneous and asymmetric layups. They introduced the layup $[90_n/0_n]$ as the layup which has the most deformation. Also, the results obtained by Goo et al. [41]

illustrated that the most deformation takes place in the non-homogeneous and asymmetrical layering which their results have appropriate consistencies with our results.

3.1.2 Effect of layer thickness

In this section, the effect of three layer thicknesses of 0.1, 0.2, and 0.3 mm is investigated on the bending deformation in the $[90_n/0_n]$ layup. This comparison was done for the total thickness of the specimens being 1.2 mm and the consistent ratio of 0° and 90° layers. The different layer thicknesses can be observed in Fig. 8. The constant printing conditions were examined in Table 1. The values of deformation percentages of striped-shape PLA specimens can be observed in Table 4 at different layer thicknesses of the specimens.

Table 4 Bending deformation percentage of striped-shape PLA specimens for total layer thickness of 1.2 mm

Layer thickness (mm)	Layup	Without wall	With wall
		Deformation percentage ± SDV (%)	Deformation percentage ± SDV (%)
0.1	$[90_6/0_6]$	-69.97±3.1	-8.34±0.1
0.2	$[90_3/0_3]$	-6.29±0.2	-3.56±0.3
0.3	$[90_2/0_2]$	-3.55±0.27	-2.61±0.21

The experimental results indicate an inverse relationship between the deformation percentage and the layer thickness for both sets of specimens; with and without wall. Specifically, as the layer thickness increases, the deformation rate decreases by approximately 89.85% and 68.7% for specimens without the wall and the ones with the wall, respectively. Reducing the layer thickness results in less material being extruded from the nozzle, allowing for faster cooling of the printed layers. Consequently, thin layers enable more stored pre-strain and show more deformation through applying stimulus. It can also be noted that increasing the layer thickness reduces the flexibility, resulting in decreased deformation. In terms of comparing specimens with and without wall, the presence of a wall acts as a robust frame, effectively preventing deformation. Hence, less deformation is observed in specimens with wall. Fig. 9 illustrates the actual bending deformation of the printed specimens without wall effect across various layer thicknesses. Video 1 in supplementary data shows the behavior of the printed specimens over time. Previous studies in [37] and [40] coincide with the results obtained in this section.

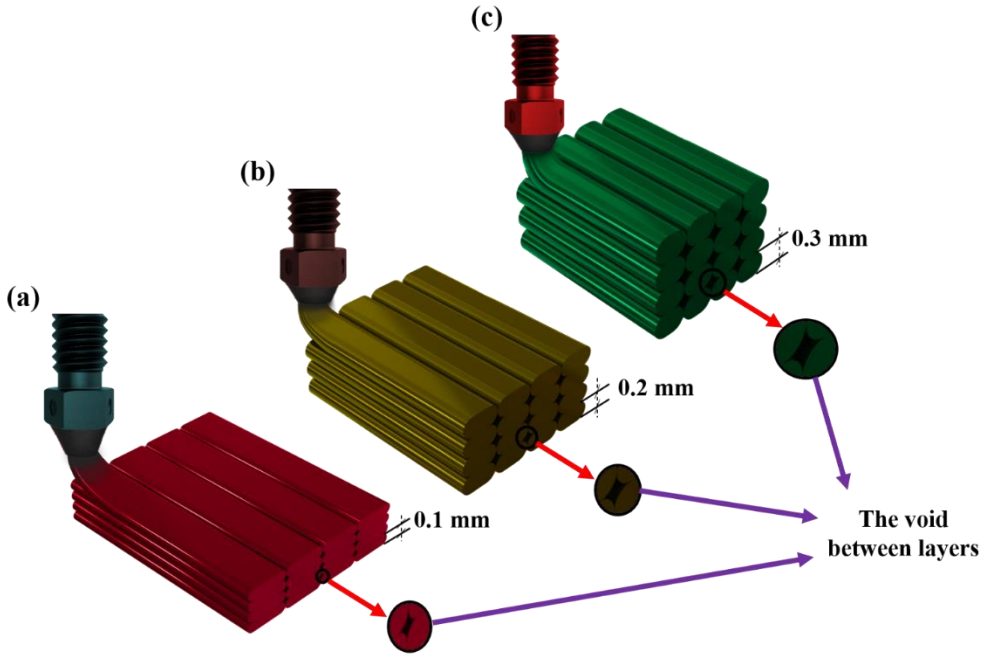

Fig. 8 Void creation in various layer thicknesses of (a) 0.1 mm, (b) 0.2 mm, and (c) 0.3 mm

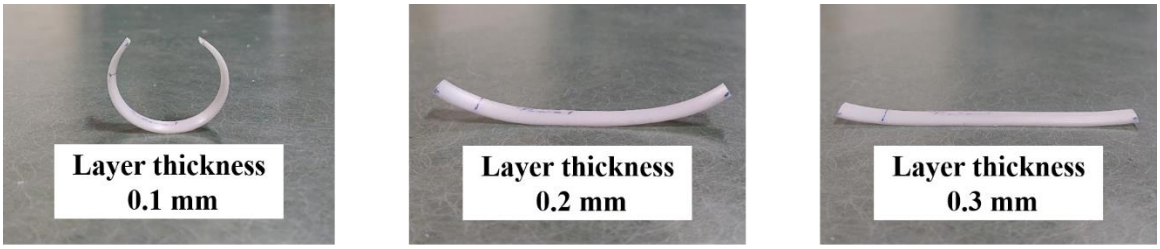

Fig. 9 The final deformation of 3D-printed shape-morphing PLA material with different layer thicknesses

3.1.3 Effect of printing speed

One of the most effective parameters for bending deformation is the printing speed. In this subsection, the effect of three printing speeds of 20, 40, and 60 mm/s is investigated on the bending deformation and other process parameters remain constant and their values are reported in Table 1. According to the results shown in Fig. 10a, by increasing the printing speed, the printed specimens are less exposed to the nozzle heat and the hot materials coming out, which leads to the rapid cooling of the specimens after printing. Also, the higher the printing speed, the higher the elongation of the material in each layer (see Fig. 11). Thus, more residual stress is created in the printed specimens. All these factors cause the stored

pre-strain to escalate by enhancing the printing speed in the printed specimens and providing larger deformation. Also, it is observed that reducing the printing speed results in a decrease in the percentage of deformation for both parts with and without wall. Specifically, the deformation percentage decreases by approximately 57.75% for specimens without wall and by 28.01% for specimens with wall. This disparity in deformation between the cut and uncut specimens highlights the influence of the wall and the non-uniform printing speed on the two series of printed specimens. Fig. 10b displays the final deformation of the no-wall specimens at various printing speeds.

Hu et al. [35] conducted a study on the strip-shaped specimens made of an SMP printed at different printing speeds of 20, 30, 40, and 50 mm/s. The layers were printed only in the length direction of the specimens. Their results showed that by increasing the printing speed, the larger deformation can be achieved. In another study, Bodaghi et al. [36] also perused the influence of printing speed and claimed that by enhancing the printing speed from 20 to 70 mm/s in the printed specimens, large deformation can be obtained, and their results were consistent with our results. Video 2 in supplementary data demonstrates the bending deformation of the 3D-printed specimens over time.

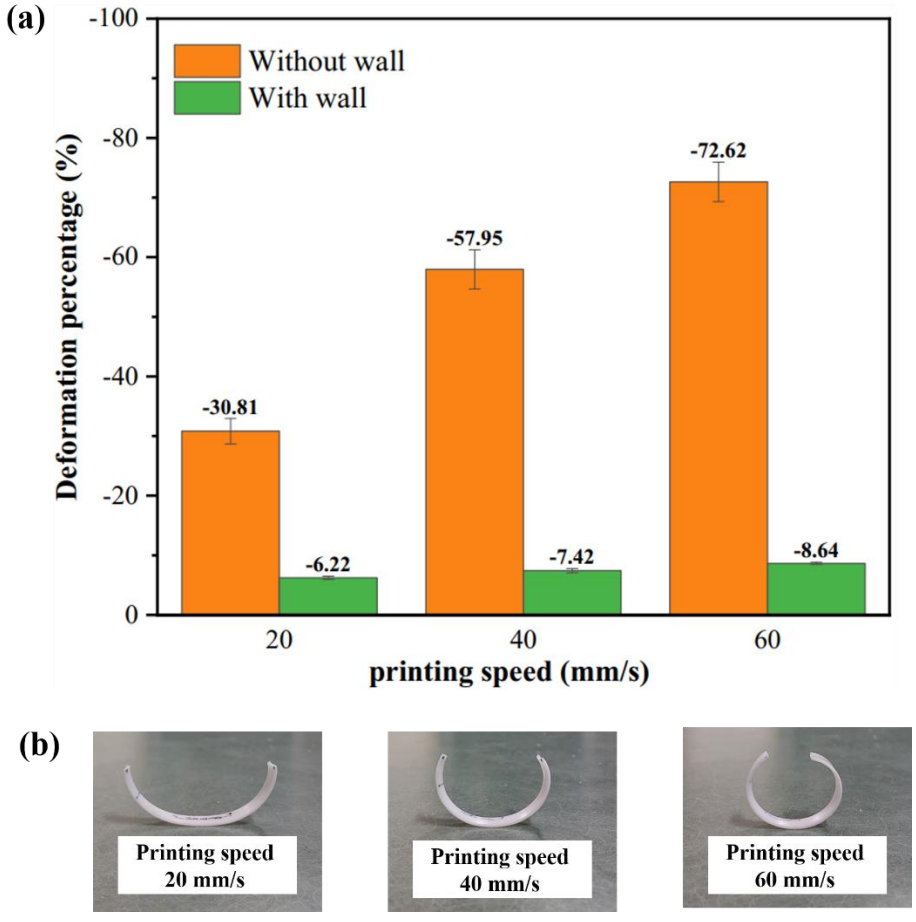

Fig. 10 (a) The values and (b) the shapes of the final deformation of PLA materials at various printing speeds

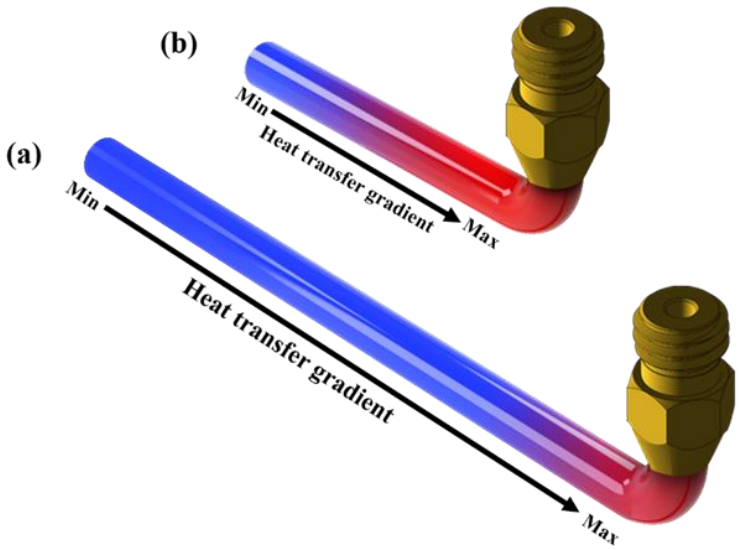

Fig. 11 The schematic of the heat transfer gradient and elongation of materials during a constant time at (a) high speed and (b) low speed

3.1.4 Effect of nozzle temperature

According to the constant printing parameters, the effect of nozzle temperature is studied at three levels of 190, 200, and 210°C. The results depicted in Fig. 12 demonstrate the impact of nozzle temperature on the bending deformation of strip-shaped specimens with and without wall. As the nozzle temperature grows, the deformation percentage declines by approximately 83.22% for the wall-less specimens and 62.44% for the with wall specimens. Accordingly, more heat flux is transferred to the printed specimens when they are printed simultaneously and much more time is needed for the cooling of specimens. This increase in the cooling time of the printed specimens causes the loss of a large amount of pre-strain created during the printing process, which ultimately reduces the amount of final deformation. The obtained results in this research have a convenient consistency with a previous study carried out by Bodaghi et al. [38].

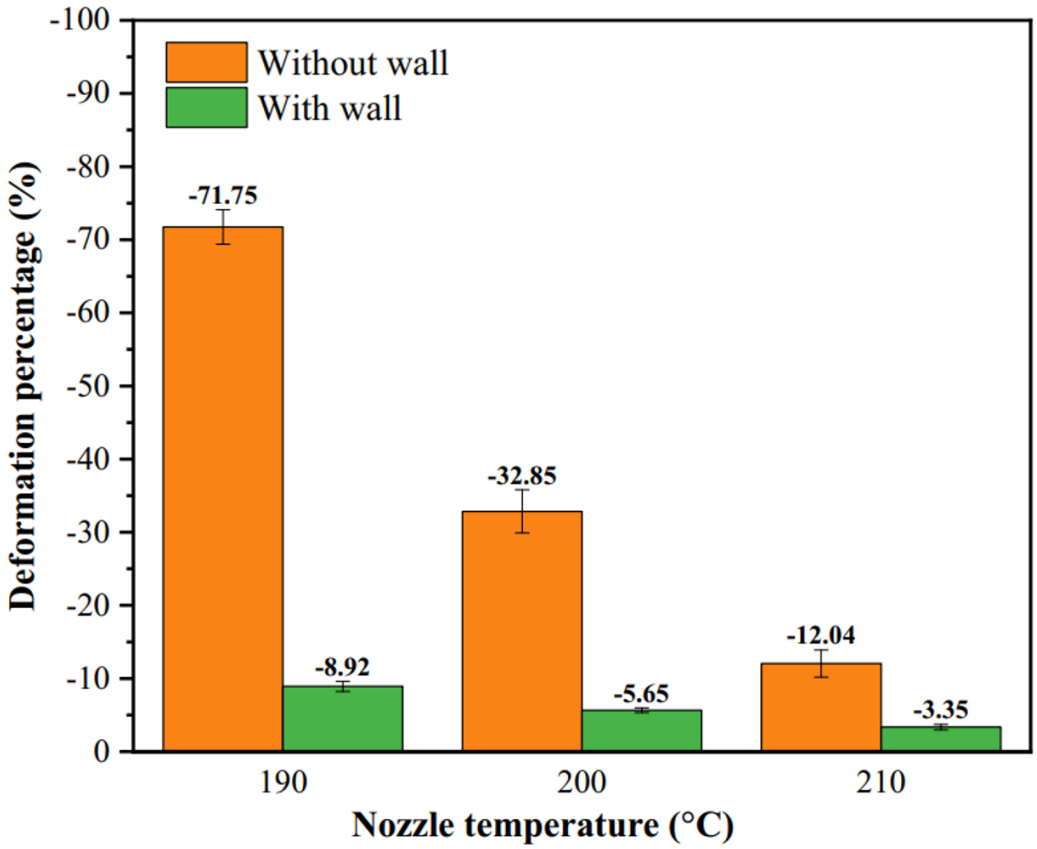

Fig. 12 The amount of final deformation of printed specimens with different nozzle temperatures

3.1.5 Effect of nozzle diameter

In this section, the nozzle diameter has been examined at three levels of 0.4, 0.6 and 0.8 mm. It was observed that the nozzle diameter can affect both the amount of deformation. The obtained results Fig. 13 demonstrate that the deformation percentage of the wall-less specimens goes up by approximately 25.16% with the enhancement of nozzle diameter. There are two reasons for the enhancement of the deformation percentage through the increase of the nozzle diameter. The first one is that the injection width increases when the nozzle diameter enhances. For example, as it is revealed in Fig. 14, the material must be injected 30 times along the specimen to fill a longitudinal layer with a constant height when the nozzle diameter is 0.4 mm. Whereas, the number of injections is reduced by half for the specimen printed with a nozzle diameter of 0.8. Therefore, the printing time of the specimen reduces, and it can be cooled sooner. Accordingly, the sooner the specimen is cooled, the more the pre-strain can be stored in the specimen. The second reason is related to the heat transfer gradient of the materials coming out of the nozzle. Fig. 15 presents a schematic of the thermal gradients of output filaments from nozzles to the injected materials with diameters of 0.4, 0.6, and 0.8 mm. According to this figure, it can be observed that the output materials that are located near the nozzle opening have more heat than the materials that

exit far from the nozzle opening. Therefore, with an increase in the nozzle diameter, the temperature difference in the low-temperature zone (light blue) and high-temperature zone (dark red) increases and materials exiting the center of the nozzle diameter have a lower temperature and can store more pre-strain during the printing process. According to the mentioned reasons, it can be found that by increasing the nozzle diameter, larger deformations can be achieved.

According to Fig. 13, in the case of specimens without wall, increasing the nozzle diameter had an inverse effect on the deformation. It means that as the nozzle diameter increases, the deformation decreases by 50.29%. To understand the reduction in deformation for specimens with wall, we can consider that increasing the nozzle diameter also increases the width of the material injection by the same amount. As a result, when the nozzle diameter increases, the wall occupies a larger area. Taking this into account, it can be found that the ratios of the remaining space area in the transverse layers with wall to transverse layers without wall for nozzle diameters of 0.4 mm, 0.6 mm, and 0.8 mm are approximately 77.87, 67.72, and 56.68, respectively. From the comparison of these area ratios, it is clear that the wall area increases with the growth of the nozzle diameter. Considering that most of the occupied space in the walls is attributable to the longitudinal walls, this brings the layup $[90_6/0_6]$ closer to the layup $[90]_{12}$, resulting in less deformation.

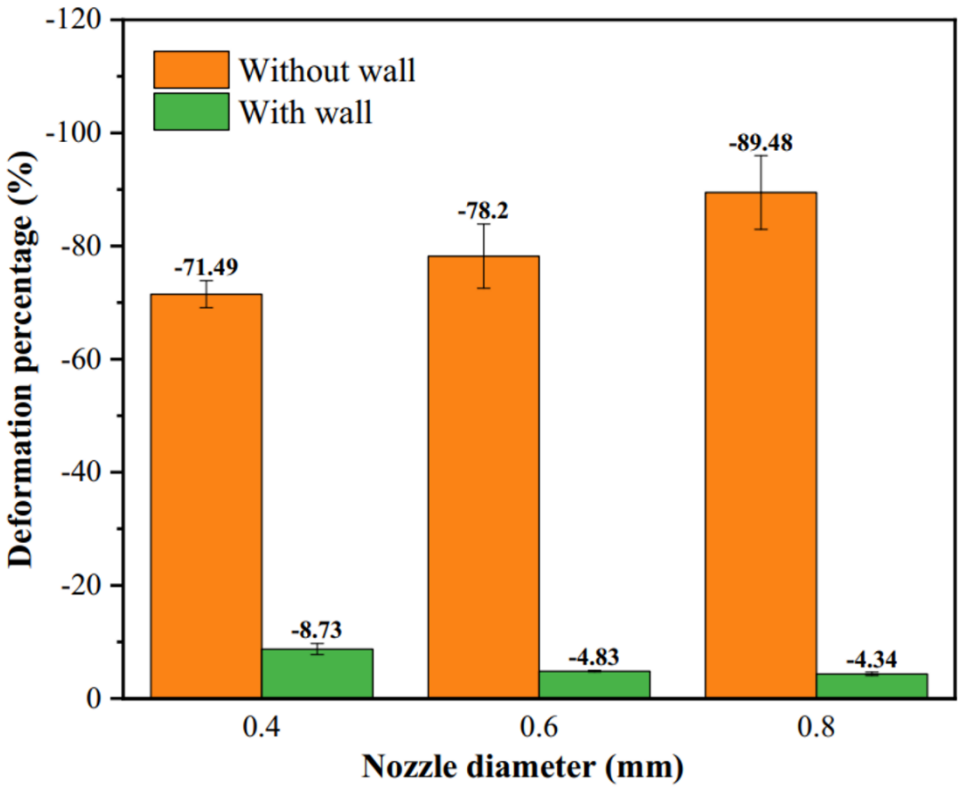

Fig. 13 Effect of nozzle diameter on the bending deformation of strip-shaped specimens

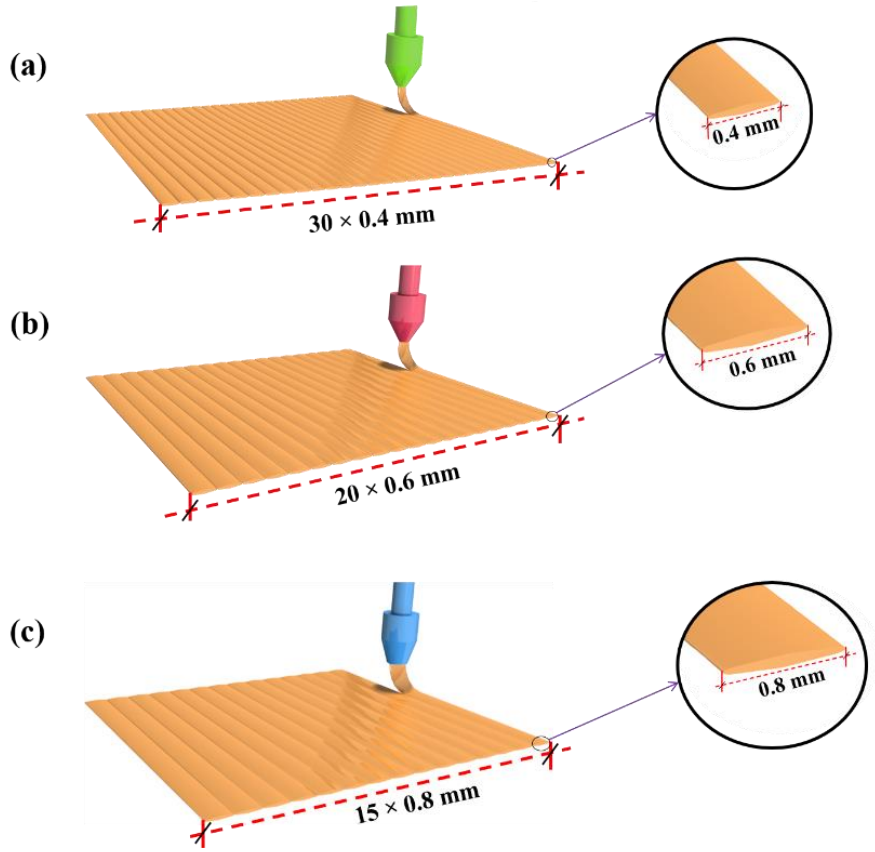

Fig. 14 The injection width of a longitudinal layer for the nozzle diameters of (a) 0.4 mm, (b) 0.6 mm, and (c) 0.8 mm

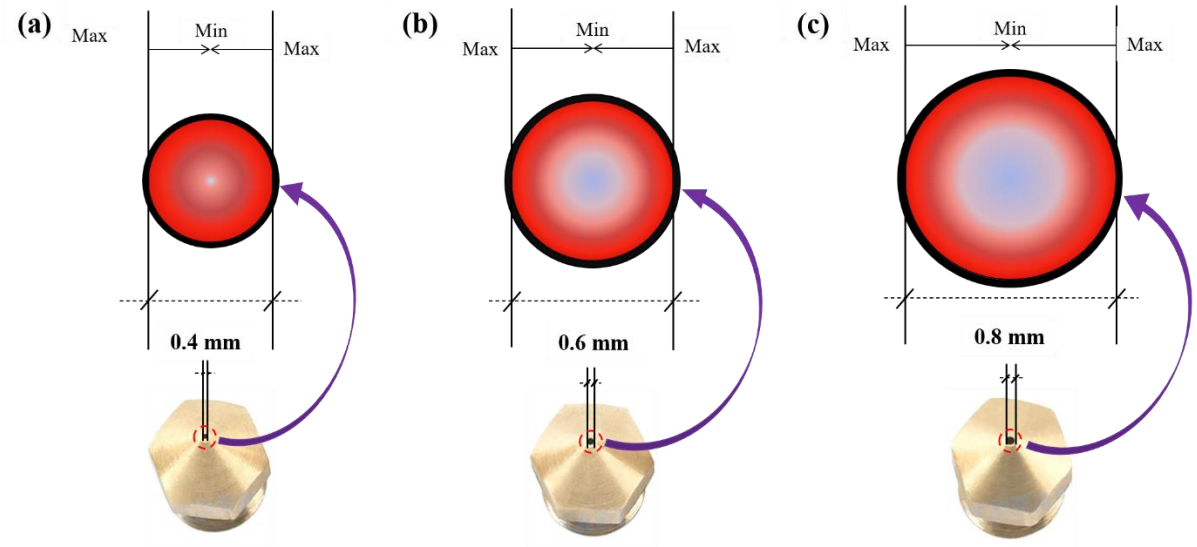

Fig. 15 Schematic of temperature gradients of output filaments in three nozzle sizes of (a) 0.4 mm, (b) 0.6 mm, and (c) 0.8 mm

3.1.6 Effect of bed temperature

In order to investigate the effect of bed temperature on the bending deformation of printed specimens, the bed temperature was investigated at three levels of 30°C, 60°C, and 80°C. These temperature levels were chosen to represent different positions (below, close, and above) relative to T_g. The findings presented in Fig. 16 indicate that the greatest deformation occurs in specimens without wall when the bed temperature is 30°C. While the lowest deformation is observed at a bed temperature of 80°C. Generally, increasing the bed temperature leads to a reduction in the stored pre-strain, ultimately resulting in decreased deformation. Two reasons can be put forth to explain this phenomenon:

- Fig. 17 illustrates the temperature distribution in 3D-printed specimens with varying bed temperatures. As the temperature increases, the upper layers are exposed to the heat from the bed, thereby reducing their stored pre-strain.
- Typically, the bed temperature is not elevated when printing structures made from PLA material. According to Fig. 18, it is evident that increasing the bed temperature significantly decreases the printing quality of specimens, causing damage to the printed specimens. Consequently, the printed specimens fail to exhibit satisfactory performance.

Furthermore, the results indicate that the difference in outcomes between specimens printed at bed temperatures of 30°C and 60°C is approximately 15.64%. This suggests that the bed temperature has lower impact compared to other printing parameters when transitioning from lower temperatures to temperatures near T_g.

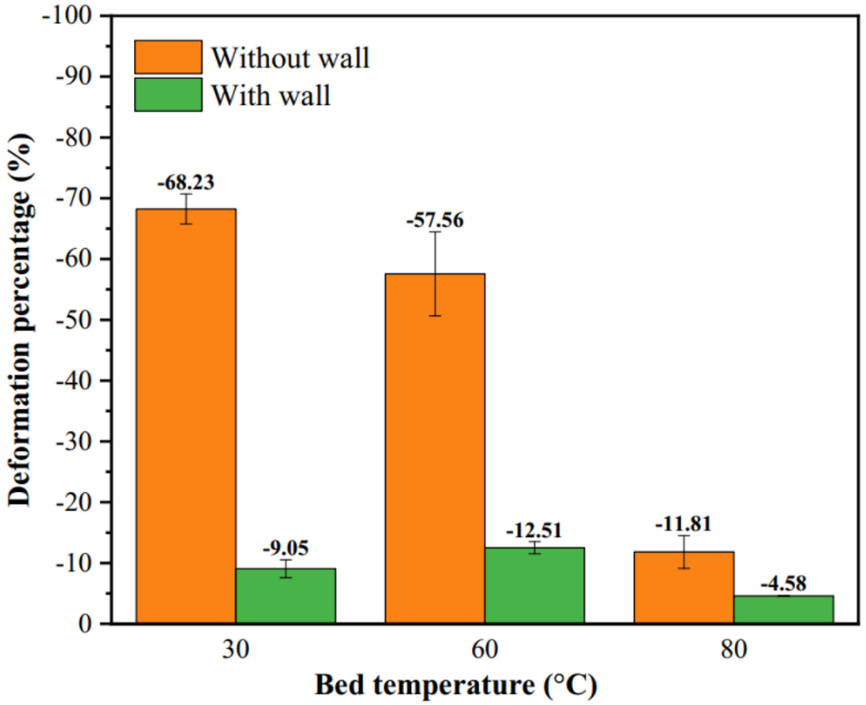

Fig. 16 Effect of bed temperature on the amount of bending deformation of strip-shaped specimens

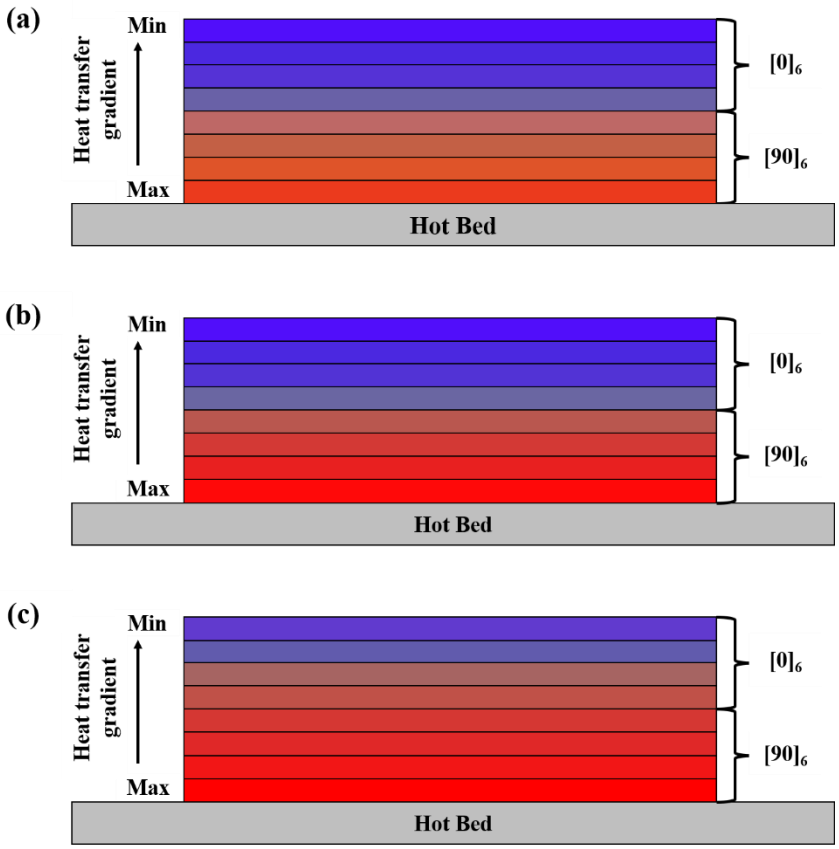

Fig. 17 Heat transfer gradient from bed temperatures of (a) 30˚C, (b) 60˚C, and (c) 80˚C

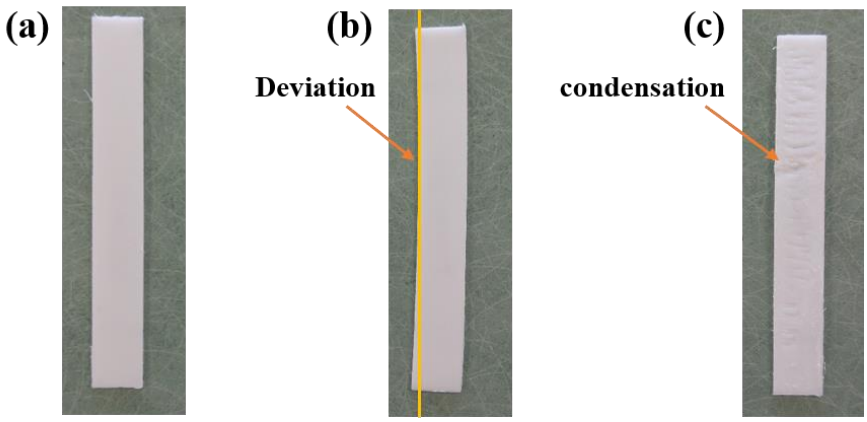

Fig. 18 Effect of bed temperature on the 3D-printed specimens quality with bed temperature (a) 30°C, (b) 60°C, and (c) 80°C

In the case of specimens with wall, as the temperature of the bed increases from 30°C to 60°C, the deformation increases and from 60°C to 80°C, the deformation decreases. This phenomenon shows the influence of the wall on the storage of non-uniform pre-strain in printed specimens.

Tezerjani et al. [42] studied the effect of bed temperature at three levels of 25, 45, and 65°C. Their results showed that the amount of deformation in printed disk-shaped PLA specimens increases with the decrease in bed temperature. This finding aligns well with the results obtained from the specimens without wall in the present study. When comparing specimens with and without wall, it becomes evident that the impact of bed temperature differs between both wall and no-wall specimens. Therefore, it can be inferred that the bed temperature may have varying effects on the deformation rate of thermally activated 4D printed specimens under different circumstances.

3.2 Activation time and activation temperature

The results regarding the influence of printing parameters on activation time and activation temperature are presented in Table 5. Activation time refers to the duration when the printed specimen initiates a change in shape, while activation temperature indicates the temperature at which this shape change occurs.

The results presented in Table 5 reveal that specimens with more significant shape changes have lower activation time and activation temperature, as indicated in sections 3.1.2 to 3.1.6. These findings demonstrate that increasing the layer thickness and the nozzle temperature and bed temperature lead to

higher activation time and activation temperature. Conversely, reducing the printing speed and increasing the nozzle diameter result in achieving the minimum activation time and activation temperature.

Regarding the layer thickness, it is an influential parameter in the formation of voids in FFF 3D printed specimens [45]. Increasing the layer thickness from 0.1 mm to 0.3 mm can approximately increase the void density by 97% [46]. The voids create spaces within the specimens, and air occupies these spaces. With a layer thickness of 0.3 mm, more air covers the increased void density, as higher layer thickness corresponds to higher void density in the empty space (see Fig. 8). Additionally, air has lower thermal conductivity compared to the PLA material. Consequently, the heat transfer process becomes more challenging in specimens with a layer thickness of 0.3 mm, resulting in an increase in the activation time. Furthermore, when the nozzle diameter increases from 0.4 mm to 0.8 mm while keeping the layer thickness constant, the number of these voids reduces by half. Therefore, it can be inferred that the reduction of empty spaces leads to faster activation time and activation temperature.

In general, the results indicate an inverse relationship between activation time and activation temperature and stored pre-strain. In other words, higher stored pre-strain causes the printed structures to initiate shape change more rapidly and at a lower temperature.

Table 5 Influence of process parameters on the activation time and temperature

Printing parameters	Values	Activation time (s)	Activation temperature (°C)
Layer thickness (mm)	0.1	1680	75
	0.2	1830	80
	0.3	1890	82
Printing speed (mm/s)	20	1620	77
	40	1600	76
	60	1560	74
Nozzle temperature (°C)	190	1575	74
	200	1710	77
	210	1800	80
Nozzle diameter (mm)	0.4	1560	75
	0.6	1545	74
	0.8	1530	73
Bed temperature (°C)	30	1560	74
	60	1620	76

	80	1800	84

3.3 Results of Taguchi design of experiment

To design the experiment, the four factors with the greatest effect are selected based on the results obtained in section 3.1. The purpose of this study is to optimize and evaluate the effect of these parameters on specimens without wall. Three factors, namely layup, nozzle temperature, and printing speed at three levels and layer thickness factor at two levels, are chosen for optimization. The factors consist of the following layups at three levels: P1=[$90_n/0_n$], P2=[$0_n/90_n$], and P3=[$0_{2/3n}/90_{1/3n}$]. These aforementioned layups are the layups that experienced the highest bending deformation in Section 3.1.1 and are referred to as P1=A-3, P2=A-4, and P3=A-6. The layup P3 has more asymmetry effect than the layups P1 and P2. Meanwhile, $0_{2/3n}/90_{1/3n}$ in the layup P3 illustrates that the number of the 0° layers is two-thirds of the number of all layers. Also, the number of the 90° layers is one-third of the number of all layers. The nozzle temperature is set at three levels: 190°C, 200°C, and 210°C, while the printing speed varies between three levels: 20 mm/s, 40 mm/s, and 60 mm/s. The layer thickness is selected at two levels: 0.1 mm and 0.2 mm. The constant parameters include a nozzle diameter of 0.4 mm, a bed temperature of 30°C, and an infill density of 100%. The absolute values of results of the Taguchi design of experiment, conducted with a minimum of three similar repetitions, are presented in Table 6.

Table 6 Taguchi test design table and the absolute value of the obtained results

Specimen	Layer thickness (mm)	Layup	Nozzle temperature (°C)	Printing speed (mm/s)	Result ± SDV
1	0.1	P1	190	20	32.24 ± 2.11
2	0.1	P1	200	40	18.49 ± 2.61
3	0.1	P1	210	60	13.52 ± 0.99
4	0.1	P2	190	20	61.33 ± 3.33
5	0.1	P2	200	40	96.14 ± 3.35
6	0.1	P2	210	60	94.57 ± 4.14
7	0.1	P3	190	40	88.21 ± 2.74
8	0.1	P3	200	60	92.65 ± 2.58
9	0.1	P3	210	20	14.62 ± 0.88
10	0.2	P1	190	60	6.45 ± 0.80
11	0.2	P1	200	20	2.34 ± 0.40

12	0.2	P1	210	40	2.05 ± 0.40
13	0.2	P2	190	40	15.33 ± 1.38
14	0.2	P2	200	60	8.64 ± 1.18
15	0.2	P2	210	20	3.21 ± 0.41
16	0.2	P3	190	60	25.12 ± 2.04
17	0.2	P3	200	20	4.26 ± 0.26
18	0.2	P3	210	40	3.81 ± 0.26

The obtained results are optimized to maximize the deformation at the selected levels using the "larger is better" criterion. The diagrams of the main effects on the percentage of bending deformation and signal-to-noise ratio (S/N) are illustrated in Fig. 19. The results presented in Fig. 19a and b exhibit a similar pattern to the findings described in section 3.1, supporting the consistency of their behavioral outcomes as explained in that section. Additionally, the S/N ratio diagram, obtained through the repetitions of the Taguchi method, was utilized to analyze the results. As indicated in Fig. 19b, the parameters of layer thickness, layup, nozzle temperature, and printing speed had significant effects on the selected surfaces, with differences of 54.32%, 35.57%, 34.35%, and 27.41%, respectively.

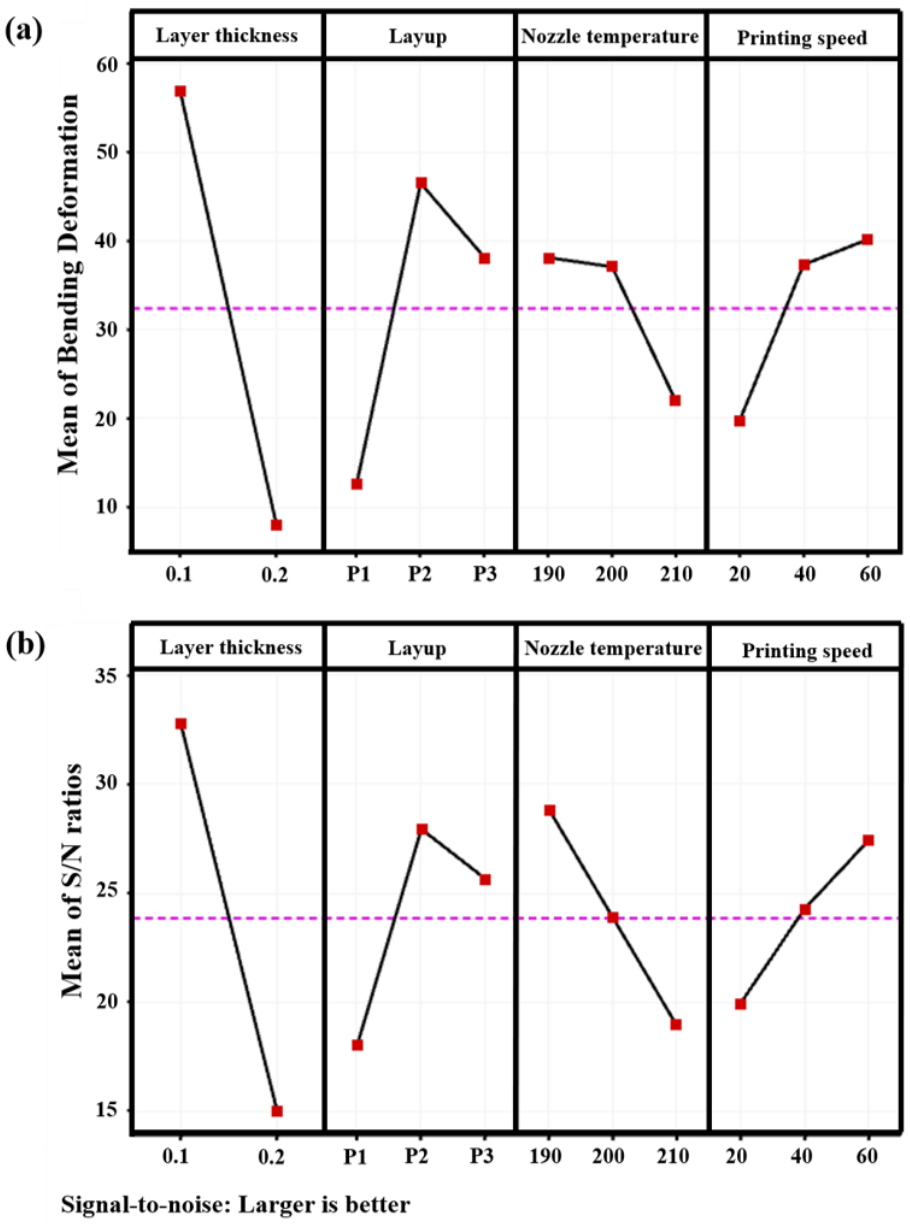

Fig. 19 The diagrams (a) the main effects on the percentage change in bending shape and (b) the signal-to-noise ratio (S/N)

Furthermore, in the S/N ratio diagram, the points located at the highest levels of each factor represent the best performance for that particular factor. The sum of the best performances of each factor illustrates the optimal state.

Taguchi design of experiment exhibits that the optimal conditions for the parameters of layer thickness, layup, nozzle temperature, and printing speed are 0.1 mm, P2, 190°C, and 60 mm/s, respectively. The Taguchi method is known for its ability to identify the best levels of factors and their effect, allowing for relatively accurate predictions of the optimal state. In this case, the Taguchi design predicted a bending

deformation value of 98.28% for the optimal state. Since the optimal state was not included in the states of Table 5, it was necessary to print specimens in order to verify the accuracy of the predicted optimal state. The deformation of the printed specimens in the optimal state was measured to be 100%, which was only 1.72% different from the predicted value by Taguchi. This level of difference is considered highly acceptable. Fig. 20 shows printed specimen with the proposed optimal parameters.

Fig. 20 The final bending deformation of optimized specimen via Taguchi method

4 Conclusion and future work

4D printing combines time with 3D printing and can turn a basic structure into an intelligent one using stimuli like heat, PH, and humidity. In engineering, material choice is important, but so is the construction process and parameters. Controlling bending, activation time, and temperature are key in managing 4D printed structures. These factors are essential to ensure the desired functionality and behavior of the printed structures. Consequently, an extensive investigation was conducted to examine the impact of various printing parameters on shape-morphing PLA specimens produced through FFF 3D printing. The parameters under scrutiny included layup, layer thickness, printing speed, nozzle temperature, bed temperature, nozzle diameter, wall printing effect, and speed non-uniformity. The study employed OFAT method and examined two sets of specimens, one without wall and another with wall.

The results revealed that the asymmetric layups exhibited significantly greater deformations compared to the symmetrical layups. Regarding the layer thickness parameter, increasing the thickness resulted in a considerable reduction in the deformation due to reduced flexibility and slower cooling, leading to a decrease in stored pre-strain. The printing speed parameter had a significant effect on the bending deformation for both specimens. By declining the printing speed from 60 to 20 mm/s, the bending deformation was reduced. This effect was observed in both wall and no-wall specimens. Additionally, higher temperatures were found to decrease stored pre-strain, consequently reducing deformation. For the specimen with wall, the bed temperature parameter demonstrated that the wall could cause a non-

uniform distribution of stored pre-strain. Regarding the nozzle diameter, deformations increased with nozzle diameter for specimens without wall, while the opposite trend was observed for specimens with wall. The study indicated that wall printing acted as a frame, preventing shape changes. Furthermore, the study findings revealed that an increase in stored pre-strain resulted in shorter activation times and lower activation temperatures for the printed structure. Eventually, the effective parameters were identified using the OFAT method, and a Taguchi design of experiment was employed to attain the optimal levels for each factor. The results demonstrated that the prediction of the optimal state via Taguchi method had a difference of less than 2% in comparison to the actual value.

Considering the numerous printing parameters that can influence the amount of bending deformation, it is crucial to select these parameters carefully to achieve the desired deformation. This careful selection ensures the avoidance of material and time wastage. As a result, future studies can concentrate on predicting the behavior of bending deformation and conducting numerical analyses.

Declarations

Funding No funding to declare.

Competing interests The authors declare no competing interests.

Author contributions *Aref Ansaripour*: Data curation, Formal analysis, Investigation, Software, and Writing original draft. *Mohammad Heidari-Rarani*: Supervision, Project administration, Conceptualization, Writing- Reviewing and Editing. *Rasoul Mahshid*: Writing- Reviewing and Editing, Supervision, Methodology. *Mahdi Bodaghi*: Writing- Reviewing and Editing, Methodology.

Data availability The raw/processed data required to reproduce these fndings can be shared on request from the authors.

References

1. Karayel E, Bozkurt Y (2020) Additive manufacturing method and different welding applications. J Mater Res Technol 9:11424–11438. https://doi.org/10.1016/j.jmrt.2020.08.039
2. Ngo TD, Kashani A, Imbalzano G, et al (2018) Additive manufacturing (3D printing): A review of materials, methods, applications and challenges. Compos Part B Eng 143:172–196. https://doi.org/10.1016/j.compositesb.2018.02.012
3. Farazin A, Mohammadimehr M (2022) Effect of different parameters on the tensile properties of

printed Polylactic acid samples by FDM: experimental design tested with MDs simulation. Int J Adv Manuf Technol 118:103–118. https://doi.org/10.1007/s00170-021-07330-w

4. Standard A (2012) ISO/ASTM 52900: 2015 Additive manufacturing General principles-terminology. ASTM F2792–10e1:

5. Mahshid R, Isfahani MN, Heidari-Rarani M, Mirkhalaf M (2023) Recent advances in development of additively manufactured thermosets and fiber reinforced thermosetting composites: Technologies, materials, and mechanical properties. Compos Part A Appl Sci Manuf 171:107584. https://doi.org/10.1016/j.compositesa.2023.107584

6. Heidari-Rarani M (2021) Residual stresses in additive manufacturing of polymers and polymer matrix composites. In: Residual Stresses in Composite Materials. Woodhead Publishing, pp 421–436

7. Heidari-Rarani M, Ezati N, Sadeghi P, Badrossamay MR (2022) Optimization of FDM process parameters for tensile properties of polylactic acid specimens using Taguchi design of experiment method. J Thermoplast Compos Mater 35:2435–2452. https://doi.org/10.1177/0892705720964560

8. Candal MV, Calafel I, Fernández M, et al (2021) Study of the interlayer adhesion and warping during material extrusion-based additive manufacturing of a carbon nanotube/biobased thermoplastic polyurethane nanocomposite. Polymer (Guildf) 224:123734. https://doi.org/10.1016/j.polymer.2021.123734

9. Rahmati A, Heidari-Rarani M, Lessard L (2021) A novel conservative failure model for the fused deposition modeling of polylactic acid specimens. Addit Manuf 48:102460. https://doi.org/10.1016/j.addma.2021.102460

10. Ali MH, Abilgaziyev A, Adair D (2019) 4D printing: a critical review of current developments, and future prospects. Int J Adv Manuf Technol 105:701–717. https://doi.org/10.1007/s00170-019-04258-0

11. Khalid MY, Arif ZU, Noroozi R, et al (2022) 4D printing of shape memory polymer composites: A review on fabrication techniques, applications, and future perspectives. J Manuf Process 81:759–797. https://doi.org/10.1016/j.jmapro.2022.07.035

12. Kuang X, Roach DJ, Wu J, et al (2019) Advances in 4D Printing: Materials and Applications. Adv Funct Mater 29:1805290. https://doi.org/10.1002/adfm.201805290

13. Ding H, Zhang X, Liu Y, Ramakrishna S (2019) Review of mechanisms and deformation

behaviors in 4D printing. Int J Adv Manuf Technol 105:4633–4649. https://doi.org/10.1007/s00170-019-03871-3

14. Megdich A, Habibi M, Laperrière L (2023) A review on 4D printing: Material structures, stimuli and additive manufacturing techniques. Mater Lett 337:133977. https://doi.org/10.1016/j.matlet.2023.133977

15. Qu H (2020) Additive manufacturing for bone tissue engineering scaffolds. Mater Today Commun 24:101024. https://doi.org/10.1016/j.mtcomm.2020.101024

16. Momeni F, M.Mehdi Hassani.N S, Liu X, Ni J (2017) A review of 4D printing. Mater Des 122:42–79. https://doi.org/10.1016/j.matdes.2017.02.068

17. Zawaski CE, Wilts EM, Chatham CA, et al (2019) Tuning the material properties of a water-soluble ionic polymer using different counterions for material extrusion additive manufacturing. Polymer (Guildf) 176:283–292. https://doi.org/10.1016/j.polymer.2019.06.005

18. Zhao W, Zhu J, Liu L, et al (2023) A bio-inspired 3D metamaterials with chirality and anti-chirality topology fabricated by 4D printing. Int J Smart Nano Mater 14:1–20. https://doi.org/10.1080/19475411.2022.2120110

19. Pei E, Loh GH (2018) Technological considerations for 4D printing: an overview. Prog Addit Manuf 3:95–107. https://doi.org/10.1007/s40964-018-0047-1

20. Ansaripour A, Heidari-Rarani M, Mahshid R (2023) A review on 4D printing of polymers and polymer composites. J Sci Technol Compos 10:2147–2165. https://doi.org/10.22068/jstc.2023.1999336.1831

21. Khalid MY, Arif ZU, Ahmed W, et al (2022) 4D printing: Technological developments in robotics applications. Sensors Actuators A Phys 343:113670. https://doi.org/10.1016/j.sna.2022.113670

22. Raina A, Haq MIU, Javaid M, et al (2021) 4D Printing for Automotive Industry Applications. J Inst Eng Ser D 102:521–529. https://doi.org/10.1007/s40033-021-00284-z

23. Subeshan B, Baddam Y, Asmatulu E (2021) Current progress of 4D-printing technology. Prog Addit Manuf 6:495–516. https://doi.org/10.1007/s40964-021-00182-6

24. Champeau M, Heinze DA, Viana TN, et al (2020) 4D Printing of Hydrogels: A Review. Adv Funct Mater 30:1910606. https://doi.org/10.1002/adfm.201910606

25. Farid MI, Wu W, Liu X, Wang P (2021) Additive manufacturing landscape and materials perspective in 4D printing. Int J Adv Manuf Technol 115:2973–2988.

https://doi.org/10.1007/s00170-021-07233-w

26. Zeng C, Liu L, Du Y, et al (2023) A Shape-Memory Deployable Subsystem with a Large Folding Ratio in China's Tianwen-1 Mars Exploration Mission. Engineering 28:49–57. https://doi.org/10.1016/j.eng.2023.01.005

27. Mehrpouya M, Vahabi H, Janbaz S, et al (2021) 4D printing of shape memory polylactic acid (PLA). Polymer (Guildf) 230:124080. https://doi.org/10.1016/j.polymer.2021.124080

28. Alikarami N, Abrisham M, Huang X, et al (2022) Compatibilization of PLA grafted maleic anhydrate through blending of thermoplastic starch (TPS) and nanoclay nanocomposites for the reduction of gas permeability. Int J Smart Nano Mater 13:130–151. https://doi.org/10.1080/19475411.2022.2051639

29. DeStefano V, Khan S, Tabada A (2020) Applications of PLA in modern medicine. Eng Regen 1:76–87. https://doi.org/10.1016/j.engreg.2020.08.002

30. Shao L-H, Zhao B, Zhang Q, et al (2020) 4D printing composite with electrically controlled local deformation. Extrem Mech Lett 39:100793. https://doi.org/https://doi.org/10.1016/j.eml.2020.100793

31. Wu J, Zhao Z, Kuang X, et al (2018) Reversible shape change structures by grayscale pattern 4D printing. Multifunct Mater 1:15002. https://doi.org/10.1088/2399-7532/aac322

32. Akbari S, Sakhaei AH, Kowsari K, et al (2018) Enhanced multimaterial 4D printing with active hinges. Smart Mater Struct 27:65027. https://doi.org/10.1088/1361-665X/aabe63

33. Alshahrani HA (2021) Review of 4D printing materials and reinforced composites: Behaviors, applications and challenges. J Sci Adv Mater Devices 6:167–185. https://doi.org/10.1016/j.jsamd.2021.03.006

34. Xin X, Liu L, Liu Y, Leng J (2020) 4D Printing Auxetic Metamaterials with Tunable, Programmable, and Reconfigurable Mechanical Properties. Adv Funct Mater 30:2004226. https://doi.org/10.1002/adfm.202004226

35. Hu GF, Damanpack AR, Bodaghi M, Liao WH (2017) Increasing dimension of structures by 4D printing shape memory polymers via fused deposition modeling. Smart Mater Struct 26:125023. https://doi.org/10.1088/1361-665X/aa95ec

36. Bodaghi M, Noroozi R, Zolfagharian A, et al (2019) 4D printing self-morphing structures. Materials (Basel) 12:1353. https://doi.org/10.3390/ma12081353

37. Van Manen T, Janbaz S, Zadpoor AA (2017) Programming 2D/3D shape-shifting with hobbyist 3D printers. Mater Horizons 4:1064–1069. https://doi.org/10.1039/c7mh00269f

38. Bodaghi M, Damanpack AR, Liao WH (2017) Adaptive metamaterials by functionally graded 4D printing. Mater Des 135:26–36. https://doi.org/10.1016/j.matdes.2017.08.069

39. Kačergis L, Mitkus R, Sinapius M (2019) Influence of fused deposition modeling process parameters on the transformation of 4D printed morphing structures. Smart Mater Struct 28:105042. https://doi.org/10.1088/1361-665X/ab3d18

40. Yu Y, Liu H, Qian K, et al (2020) Material characterization and precise finite element analysis of fiber reinforced thermoplastic composites for 4D printing. CAD Comput Aided Des 122:102817. https://doi.org/10.1016/j.cad.2020.102817

41. Goo B, Hong CH, Park K (2020) 4D printing using anisotropic thermal deformation of 3D-printed thermoplastic parts. Mater Des 188:108485. https://doi.org/10.1016/j.matdes.2020.108485

42. Tezerjani SMD, Yazdi MS, Hosseinzadeh MH (2022) The effect of 3D printing parameters on the shape memory properties of 4D printed polylactic acid circular disks: An experimental investigation and parameters optimization. Mater Today Commun 33:104262. https://doi.org/10.1016/j.mtcomm.2022.104262

43. Alshebly YS, Nafea M, Mustapha KB, et al (2022) Variable stiffness 4D printing. Smart Mater Addit Manuf Vol 2 4D Print Mech Model Adv Eng Appl 407–433. https://doi.org/10.1016/B978-0-323-95430-3.00015-4

44. Jamshidi M, Salimi Nezhad I, Golzar M, Behravesh AH (2021) Investigation of the Effect of 3D printing parameters on shape-shifting of flat sturctures to Three-Dimensional Shapes. J Sci Technol Compos 7:1271–1278. https://doi.org/10.22068/jstc.2021.141438.1693

45. Sun X, Mazur M, Cheng CT (2023) A review of void reduction strategies in material extrusion-based additive manufacturing. Addit Manuf 67:103463. https://doi.org/10.1016/j.addma.2023.103463

46. Garzon-Hernandez S, Garcia-Gonzalez D, Jérusalem A, Arias A (2020) Design of FDM 3D printed polymers: An experimental-modelling methodology for the prediction of mechanical properties. Mater Des 188:108414. https://doi.org/10.1016/j.matdes.2019.108414